JOURNAL OF AGRICULTURAL AND FOOD CHEMISTRY

Article

Cite This: J. Agric. Food Chem. 2019, 67, 10713−10725

pubs.acs.org/JAFC

Converting Peanut Protein Biomass Waste into "Double Green" Meat Substitutes Using a High-Moisture Extrusion Process: A Multiscale Method to Explore a Process for Forming a Meat-Like Fibrous Structure

Jinchuang Zhang,[†] Li Liu,[†] Yuanrong Jiang,[‡] Shah Faisal,[†] Linlin Wei,[§] Chunjie Cao,[∥] Wenhui Yan,[⊥] and Qiang Wang*,[†]

[†]Institute of Food Science and Technology, Chinese Academy of Agriculture Sciences/Key Laboratory of Agro-Products Processing, Ministry of Agriculture and Rural Affairs, Beijing 100193, China

[‡]Wilmar (Shanghai) Biotechnology Research & Development Center Co., Ltd, Pudong New District, Shanghai 200137, China

[§]Bruker (Beijing) Scientific Technology Co., Ltd, Minhang District, Shanghai 200233, China

[∥]Carl Zeiss (Shanghai) Co., Ltd., 60 Mei Yue Road, Pilot Free Trade Zone, Shanghai 200131, China

[⊥]Hunan Fumach Foodstuff Eng & Tech, Co., Ltd, Kaifu District, Changsha 410153, China

Supporting Information

ABSTRACT: Converting peanut protein biomass waste into environmentally friendly meat substitutes by a high-moisture extrusion process can help solve both resource and waste problems and be "double green". A multiscale method combined with some emerging techniques such as atomic force microscopy-based infrared spectroscopy and X-ray microscopy was used to make the whole extrusion process visible to show the process of forming a meat-like fibrous structure using two-dimensional and three-dimensional perspectives. The results showed that the protein molecules underwent dramatic structural changes and unfolded in the extruder barrel, which created favorable conditions for molecular rearrangement in the subsequent zones. It was confirmed that the meat-like fibrous structure started to form at the junction of the die and the cooling zone and that this structure was caused by the phase separation and rearrangement of protein molecules in the cooling zone. Moreover, the interactions between hydrogen bonds and disulfide bonds formed in the cooling zone maintained the meat-like fibrous structure with an α-helix > β-sheet > β-turn > random coil. Of the two main peanut proteins, arachin played a greater role in forming the fibrous structure than conarachin, especially those subunits of arachin with a molecular weight of 42, 39, and 22 kDa.

KEYWORDS: *peanut protein biomass waste, high-moisture extrusion process, meat substitutes, meat-like fibrous structure, multiscale method*

1. INTRODUCTION

The waste of natural resources must attract our attention, especially protein resources.[1] With the world population estimated to reach 9 billion by 2050, one of the biggest challenges to global food security is ensuring that protein requirements can be met in a way that is affordable, healthy, and environmentally responsible.[2] Several global studies have suggested that dietary changes, such as reducing the consumption of animal-sourced food and adopting plant-based options, can reduce environmental impact in the form of reducing greenhouse gas emissions, water use, land use, and the risk of diet-related noncommunicable diseases.[3,4] A sustainable alternative to intensive meat production would be the development of plant protein-based environmentally friendly meat substitutes with a meat-like fibrous structure. High-moisture extrusion technology for moisture contents higher than 40% has the advantages of lower energy input, no waste discharge, high efficiency, and higher quality of the texturized products, which should be considered one of the best choices.[5,6] However, the market for plant protein-based meat substitutes is still quite small, probably because the meat substitutes currently available do not meet consumer preferences regarding sensory quality.[7] To obtain a larger market share, plant protein-based meat substitutes need to be comparable with the real animal meat products in terms of flavor, texture, and overall organoleptic acceptability.[6]

Peanut protein biomass waste, obtained as a byproduct of the edible oil industry, has become the third largest plant protein source in the world with a protein content greater than 55%. More than 5 million tons of peanut protein biomass wastes are produced globally every year with the most being used as animal feed, which leads to a lower added value than that of foods.[8] Peanut protein, mainly arachin and conarachin, has a higher digestibility (~90%), no flatulence factor, and bean flavor, so helps overcome the disadvantages of consuming soybean protein. Additionally, according to the protein digestibility corrected amino acid score, peanut protein and

Received: April 30, 2019
Revised: July 21, 2019
Accepted: August 27, 2019
Published: August 27, 2019

Downloaded via CHINESE ACADEMY AGRICULTURAL SCI on December 6, 2019 at 03:53:44 (UTC).
See https://pubs.acs.org/sharingguidelines for options on how to legitimately share published articles.

ACS Publications © 2019 American Chemical Society

DOI: 10.1021/acs.jafc.9b02711
J. Agric. Food Chem. 2019, 67, 10713−10725

other legume proteins are nutritionally equivalent to meat and eggs for human growth and health.[8] By using biowaste feedstock (including agricultural waste, food-processing waste, municipal solid waste, and sewage sludge) to make bio-based food products, it can help solve both resource and waste problems and be "double green".[1]

The extrusion process can be considered as a complicated multi-input−output system, in which the feed components undergo complex physical and chemical changes and exit the extruder as a transformed product.[9] Several studies have focused on optimizing the extrusion conditions, characterizing the extrudate, or investigating the correlation between process, system, and product parameters.[5,10−12] To get more information during the extrusion process, a dead-stop operation, where the process is intentionally halted after reaching a steady state, has been used to collect the samples in the extruder barrel and the die.[10] Some studies have reported that the molecular weight of the soybean protein started changing in the mixing zone of the extruder, with new disulfide bonds being formed in the die, thus promoting the formation of the fibrous structure in the cooling zone.[13] However, the resulting images provided very little information and controlling the extrusion process precisely is still very challenging with the extrusion process itself being considered as a "black box".[6] To obtain a full understanding of the state of the raw material during the extrusion process, some emerging techniques such as atomic force microscopy-based infrared spectroscopy (AFM-IR) and X-ray microscopy should be helpful.[14,15]

Therefore, the objectives of the present study are to design a high-moisture extrusion process to convert the peanut protein biomass waste into meat substitutes; to understand the behavior of the "black box" for the high-moisture extrusion process using a multiscale method from two-dimensional (2D) and three-dimensional (3D) perspectives; to differentiate the flowing behavior combining with the thermal transition and decomposition properties of the peanut protein samples in each extrusion zone; and to examine the changes in protein conformation such as protein−protein interactions, in the molecular weight distribution, and in the secondary structure during the high-moisture extrusion process.

2. MATERIALS AND METHODS

2.1. Materials. Peanut protein biomass waste containing a protein content of 60.75 ± 0.748 g/100 g (dry basis) was supplied by Qingdao Longevity Food Co., Ltd. (Qingdao, China), shown in Table S1.

2.2. High-Moisture Extrusion Process. All of the extrusion experiments were conducted using a co-rotating and intermeshing twin-screw food extruder (FMHE36-24, FUMACH, China) (Figure S1). The peanut protein biomass waste was fed into the extruder at a constant speed of 6 kg/h (dry basis). On the basis of the preliminary experiments and the working stability of the extruder,[16] the feed moisture was selected as 55% (dry basis), the screw speed was 210 rpm, and the extruder barrel temperatures were kept at 60, 90, 155, 155, and 110 °C from the first zone to the fifth zone, respectively. A long cooling die was connected to the end of the extruder barrel and kept at 70 °C by running water. After reaching the steady state, as indicated by constant values for motor torque and die temperature, the extrusion operation was intentionally shut down (dead-stop) for sample collection according to Chen et al.[9]

2.3. Textural Properties of the Fresh Extrudates (Meat Substitutes). The textural properties of the fresh extrudates including the hardness, springiness, tensile strength, lengthwise strength, crosswise strength, and fibrous degree (ratio of the crosswise to lengthwise strength) were measured with a Texture Analyzer (TA.XT2, Stable Micro Systems, UK) according to Fang et al.[17]

2.4. Camera, X-ray Microscope, Scanning Electron Microscope, and AFM-IR Analysis for the Structural Observation of Peanut Protein in Each Zone. The macrostructure of the fresh samples from the different zones was photographed using a camera (D7200, Nikon Corp., Tokyo, Japan). The obtained samples were first freeze-dried to remove the water, then scanned using a Zeiss Xradia 510 Versa X-ray microscope [Carl Zeiss (Shanghai) Co. Ltd., Shanghai, China], pausing at discrete angles to collect 2D projection images, which were then combined to produce a 3D reconstruction of the samples' volume dataset. All the samples were imaged with 0.7 μm/voxel, field of view of 0.7 × 0.7 mm in 5 h. The X-ray tomography data were processed using ORS Visual SI software (ORS Inc., Montreal, Canada).

The microstructure of the extrudates was studied by scanning electron microscopy (SU8010, Hitachi Ltd., Tokyo, Japan). Frozen samples were kept for 30 min at room temperature prior to sample preparation. Structures were cut into small rectangles (the longest edge was 8 mm) and mounted in a glutaraldehyde solution (2.5 vol %) for 48 h. The next day, the sample was rinsed with cold phosphate buffer (0.1 M) and followed by a secondary fixation in osmium tetroxide (1%) for 2 h. Then, the samples were critical point dried in CO_2. Dehydrated samples were coated with gold particles with a sputter coater (IB-5, Hitachi Ltd., Tokyo, Japan). The images of the samples were taken with a scanning electron microscope at magnifications of ×300 and ×1500, respectively.

We adopted the semi-thin sectioning method to obtain slices of fresh samples approximately 300 nm thick. The AFM-IR measurements were made using a nanoIR2 system (Bruker, Billerica, MA, USA) equipped with a multichip pulsed QCL laser (MIRcat, DRS Daylight Solutions Inc., San Diego, CA, USA) ranging from 910 to 1950 cm^{-1}. At least three points were selected to detect the nano-IR information for each slice.

2.5. DSC, TG, and DTG (Derivative thermogravimetric curves) Measurements. The freeze-dried samples were ground, then passed through an 80-mesh sieve. One gram of the powder sample was weighed into a 4 mL centrifuge tube; then, deionized water was added until the water content of the mixture was 55% (w/w), the preferred moisture level for extrusion.[16] The differential scanning calorimetry (DSC) curves were obtained using a Thermal Analysis Systems Model Q-200 (TA Instruments, New Castle, DE, USA). The samples were first conditioned in a hermetic high-pressure capsule kit (TA Instruments), weighed (8−10 mg) using a precision balance (±0.01 mg, Analytical Plus, Mettler-Toledo International Inc., Columbus, OH, USA), then heated at a rate of 5 °C/min from 25 to 130 °C in an inert atmosphere (50 mL/min of dry N_2).

Nonisothermal degradation measurements were made using TG/DTA (thermogravimetric/differential thermal analysis; Pyris Diamond, PerkinElmer Inc., Waltham, MA, USA). Tests were run from room temperature up to 500 °C at a heating rate of 10 °C/min in a nitrogen atmosphere (50 mL/min) to avoid thermo-oxidative reactions. The mass loss curves were divided into five parts and the residue mass and peak temperature were recorded according to our previous study.[18]

2.6. Rheological Measurements. The samples in this section were reconstituted at 20% (w/w) concentration in deionized water and gently stirred for 2 h or until dissolution was completed and then stored overnight at 4 °C prior to testing. The steady shear test was performed at 25 °C over a shear rate range of 1−100 s^{-1} using a rheometer (Physica MCR 301, Anton Paar, Austria) with aluminum parallel plate geometry (50 mm diameter, 1 mm gap). A thin layer of silicone oil was added on the edge of the sample to avoid evaporation. All the tests were carried out allowing the sample to equilibrate for 2 min to eliminate the effect of loading of the sample on the plate. Shear stress (τ), shear rate (γ), and apparent viscosity (η) were measured in these tests.[19] The steady shear flow curves were fitted by power law according to eq 1. The flow behavior index (n) and consistency coefficient (K) were reported.

DOI: 10.1021/acs.jafc.9b02711
J. Agric. Food Chem. 2019, 67, 10713−10725

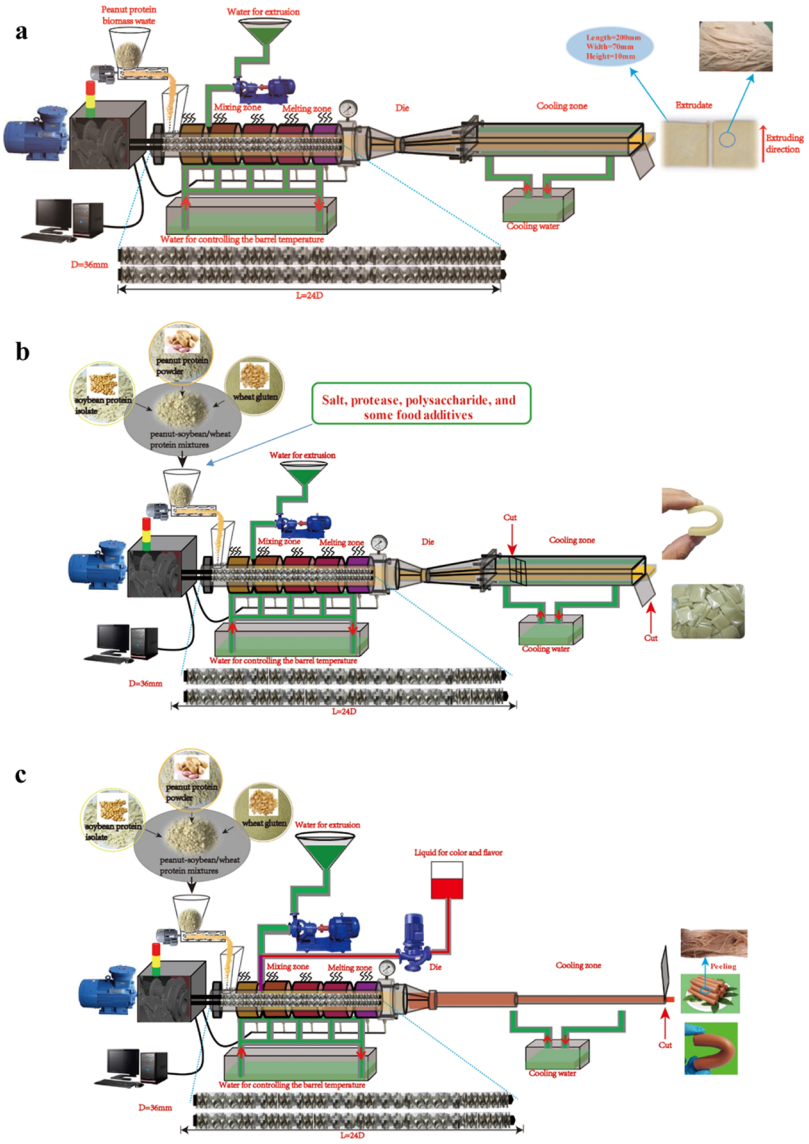

Figure 1. High-moisture extrusion process for the production of texturized-peanut protein and "double green" meat substitutes. (a) High-moisture extruded texturized-peanut protein. (b) Peanut protein-based dry tofu with high springiness. (c) Peanut protein-based vegetarian sausage.

$$\tau = K \cdot \gamma^n \quad (1)$$

The frequency sweep test was carried out at 25 °C over the angular frequency range of 0.1−100 rad/s, according to Manoi.[20] The storage modulus (G'), loss modulus (G''), and the loss tangent ($\tan \delta = G''/G'$) were measured.

2.7. Design of Extracting Systems and Determination of Protein Solubility. The protein solubility of the samples in 2.6 was analyzed using the methods of Liu et al. and Chen et al.[9,21] The buffer systems used for protein extraction were as follows: (1) 0.035 mol/L pH 7.6 phosphate buffer solution (P); (2) 8 mol/L urea in the phosphate buffer solution with pH 7.6 (P + U); (3) 0.1 mol/L 2-mercaptoethanol (2-ME) in the phosphate buffer solution with pH 7.6 (P + M); (4) 1.5 g/100 mL sodium dodecyl sulfate (SDS) in the phosphate buffer solution with pH 7.6 (P + S); (5) 8 mol/L urea and 0.1 mol/L 2-ME in the phosphate buffer solution with pH 7.6 (P + U + M); (6) 1.5 g/100 mL SDS and 8 mol/L urea in the phosphate buffer solution with pH 7.6 (P + U + S); (7) 1.5 g/100 mL SDS and 0.1 mol/L 2-ME in the phosphate buffer solution with pH 7.6 (P + S + M); and (8) 8 mol/L urea, 1.5 g/100 mL SDS and 0.1 mol/L 2-ME in the phosphate buffer solution with pH 7.6 (P + U + S + M). The total protein content of the samples was determined using the Kjeldahl method, and the soluble protein in the supernatant by the Lowery method using a microplate reader assay at 650 nm (SpectraMax, Molecular Devices, San Jose, CA, USA). The protein solubility was calculated as the ratio of soluble protein in the supernatant to the total protein in the samples. Each measurement was performed in triplicate.

2.8. Sodium Dodecyl Sulfate Polyacrylamide Gel Electrophoresis. SDS-PAGE was performed following the method of He et al.[22] Electrophoresis was conducted using the Mini-PROTEAN System (Bio-Rad, Hercules, CA, USA). Images for the protein electrophoresis spectrum were taken using an AlphaEase FC gel imaging system (Genetic Technologies Inc, Miami, FL, USA). Densitometry analysis was performed using Image Studio Lite (version 5.2, LI-COR Biosciences, Lincoln, NE, USA) for the relative quantification of the different protein bands (66, 42, 39, 38, 27, 26, 22, and 18 kDa).[23]

2.9. Fourier Transform Infrared Spectroscope Determination. Fourier transform infrared (FTIR) analysis of the samples sieved through an 80-mesh sieve were recorded using a spectrometer (TENSOR 27, Bruker, Germany). The classic KBr-disk method was used to prepare analyzed samples, by using predried 1 mg of the samples and 100 mg of KBr to obtain the compressed pellets. Spectra were collected in the 500−4000 cm^{-1} infrared spectral range at room temperature. Each spectrum was an average of 64 scans at a 4 cm^{-1}

DOI: 10.1021/acs.jafc.9b02711
J. Agric. Food Chem. 2019, 67, 10713−10725

Table 1. Textural Properties of the High Moisture Extruded-Texturized Peanut Protein, Peanut Protein-Based Dry Tofu, Peanut Protein-Based Vegetarian Sausage, and Some Commercial Meat Products[a]

samples	hardness (kg)	springiness	chewiness	tensile strength (kg)	lengthwise strength (kg)	crosswise strength(kg)	fibrous degree
high-moisture extruded-texturized peanut protein	27.80 ± 0.82	0.83 ± 0.01	13.32 ± 0.33	0.90 ± 0.11	0.44 ± 0.06	0.48 ± 0.03	1.10 ± 0.13
chicken breast meat	27.60 ± 1.64	0.67 ± 0.02	10.07 ± 1.03	-	-	-	-
beef tenderloin	15.09 ± 0.03	0.79 ± 0.05	58.21 ± 0.07	-	-	-	-
pork tenderloin	17.94 ± 7.35	0.70 ± 0.03	4.49 ± 0.01	-	-	-	-
peanut protein based-dried tofu	21.81 ± 1.09	0.95 ± 0.03	14.34 ± 0.53	-	-	-	-
commercial dried soybean tofu	5.79 ± 0.79	0.94 ± 0.02	4.58 ± 0.57	-	-	-	-
peanut protein based-vegetarian sausage	9.58 ± 0.37	0.89 ± 0.03	5.24 ± 0.22	-	0.51 ± 0.07	0.52 ± 0.07	1.03 ± 0.23
commercial ham sausage	8.10 ± 0.37	0.84 ± 0.02	4.03 ± 0.10	-	0.36 ± 0.02	0.35 ± 0.05	0.98 ± 0.09

[a]"-" means that the indicator is not detected.

resolution. The amide I band (1600−1700 cm^{-1}) in each spectrum was analyzed using Omnic software (version 8.0, Thermo Nicolet Inc., MA, USA), and PeakFit software (version 4.12, SPSS Inc., Chicago, USA) was used to analyze the secondary structure changes.

2.10. Statistical Analysis. All data were analyzed using analysis of variance (ANOVA) in the general linear model procedure of the Statistical Product and Service Solutions software package (version 19.0, SPSS Inc., Chicago, USA). The differences between group means were analyzed using Duncan's multiple-range test. Statistical significance was set at a 0.05 probability level.

3. RESULTS AND DISCUSSION

3.1. High-Moisture Extrusion Process Designed for the Production of Meat Substitutes. In the present study, we first designed the high-moisture extrusion process (Figure 1), then produced the texturized peanut protein with a rich meat-like fibrous structure using peanut protein biomass waste as the raw material. The meat-like fibrous structure was evaluated using a texture analyzer (see 2.3). The ratio of the crosswise to lengthwise strength (fibrous degree) was more than 1 (about 1.10) and the tensile strength was about 0.9 kg, which confirmed the formation of a meat-like fibrous structure in the extruding direction.[17,24] The product also exhibited values of hardness of 27.80 kg, of springiness higher than 0.83, and of chewiness of 13.32 kg, which were comparable to those of chicken breast meat (Table 1).

On the basis of these data, two new meat substitutes, a peanut protein-based dry tofu and a peanut protein-based vegetarian sausage, have been successfully developed with a higher springiness (about 0.95) and comparable textural properties, respectively compared with ham sausage (Table 1). As shown in Figure 1, these two new meat substitutes can be shaped, flavored, and colored during the extrusion process by modifying the formulation, process, and equipment, which would also greatly shorten the processing procedure without producing pollution or increasing nutrient losses. If more consumers chose these new meat substitutes, the animal killing and CO_2 production would also be reduced.

3.2. Observation of the State of Peanut Protein in Each Zone during the High-Moisture Extrusion Process from a Multiscale Perspective. The high-moisture extrusion process can be divided into six functional zones (raw material, mixing zone, melting zone, die, cooling zone, and the extrudate) for collecting samples for analysis. The images captured by the camera at a resolution of 4288 × 2848 are shown in Figure 2a. It can be seen that in the extruder barrel, the raw material was mixed with water in the mixing zone, then melted in the melting zone. As the melted material passed through the narrow-caliber die, it formed a cylindrical shape, which then became rectangular because of the shear stress provided by the cooling zone. After cooling, the surface of the extrudate became smoother.

From the X-ray tomography results (Figure 2b), the loose structure in the mixing zone exhibited a porosity of 51.84%. Under the extreme conditions (high temperature, shear force, and pressure) of reaction in the melting zone, the melted materials became closer to each other, leading to the formation of some large gelling areas and large pores, with a lower porosity of 44.90%. Later on, the melted materials were compacted in the die and these large pores disappeared. The fibers were oriented in the direction of extrusion in the cooling zone, which was consistent with previous studies.[10] In the extrudate, the fibers became thinner and cross-linked to form a reticulated fibrous structure. The increased porosity after the die should be due to the cross-linking of protein molecules and the formation of the fibrous structure, which could lead to the water redistribution.

Viewed by scanning electron microscopy (SEM) at magnifications of ×300 and ×1500, the images (Figure 2c) were consistent with the X-ray results, which showed that large protein gels were formed in the melting zone, which then became denser in the die. The SEM images also confirmed that the fiber orientation in the cooling zone exhibited a multilayered structure, which then formed the fibrous structure in the extrudate.[11]

AFM-IR analysis was used as an innovative step to determine the phase distribution of protein and other components such as lipids during the high-moisture extrusion process at a nanoscale resolution (10 nm). According to results from a preliminary test (Figure S4), IR peaks at around 1660 and 1740 cm^{-1} represent the protein and lipid information, respectively. Figure 2d shows that the protein and lipid in the material were in separate phases with a loose structure in the mixing zone, which was consistent with the X-ray image. This was probably caused by the water dilution and the mild reaction conditions in the mixing zone. Under the extreme reaction conditions of the melting zone, the proteins aggregated, which also promoted the aggregation of the lipids. Additionally, the weak IR signal of the lipid detected in the protein-rich regions may have been the result of protein−lipid interactions.[25] In the die, large protein-rich regions were found, indicating that the narrow-caliber die could promote the aggregation of protein molecules. However, in the lipid-rich regions, no IR signals of the protein were detected. This suggested that phase separation had occurred again because of

DOI: 10.1021/acs.jafc.9b02711
J. Agric. Food Chem. 2019, 67, 10713−10725

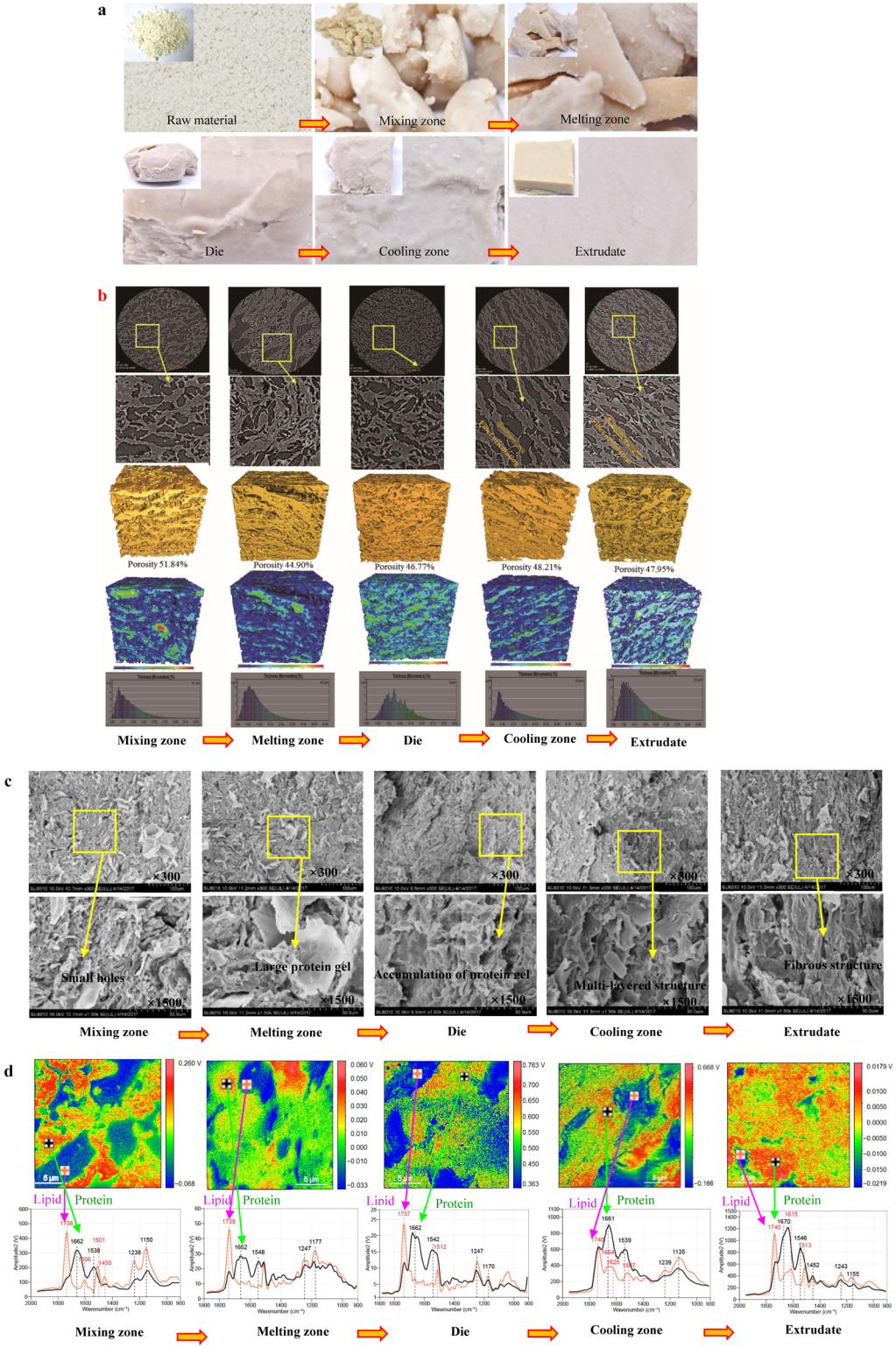

Figure 2. Multiscale structure of the peanut protein powder in each zone during the high-moisture extrusion process. (a) Images of the macrostructure taken by a camera. (b) 2D virtual slices and 3D rendering images acquired by X-ray microscopy. (c) Microstructure obtained by SEM. (d) AFM-IR analysis information for the distribution of the protein and the lipid.

thermal incompatibility and that the lipid may have been coated on the surface of the protein aggregates, which prevented the protein molecules from cross-linking.[25] In the cooling zone, the shear stress perpendicular to the extrusion direction caused the protein aggregates to be dispersed.[26] Meanwhile, the IR signal could be detected in both the protein-rich and lipid-rich regions, indicating that the lipid had been further dispersed in the multilayered structure (Figure 2c) formed by the protein aggregation.[9,27] In the extrudate, protein covered almost all the regions and the IR signals of lipid in the protein-rich regions became weak compared with those in the cooling zone. This could be explained by the fact

DOI: 10.1021/acs.jafc.9b02711
J. Agric. Food Chem. 2019, 67, 10713−10725

Table 2. Thermal Transition Properties of Peanut Protein During the High-Moisture Extrusion Process[a]

extrusion zones	conarachin		arachin	
	T_p/°C	ΔH/J g^{-1}	T_p/°C	ΔH/J g^{-1}
raw material	92.50 ± 0.55a	0.48 ± 0.02a	111.43 ± 0.16b	9.32 ± 0.18a
mixing zone	91.70 ± 2.84a	0.16 ± 0.00b	109.88 ± 0.01c	7.45 ± 0.78b
melting zone	90.39 ± 0.56ab	0.20 ± 0.01b	111.28 ± 0.99b	0.07 ± 0.00c
die	87.41 ± 0.56b	0.53 ± 0.04a	105.67 ± 0.06d	0.01 ± 0.00c
cooling zone	87.72 ± 0.60b	0.20 ± 0.03b	114.14 ± 0.09a	0.23 ± 0.01c
extrudate	89.77 ± 0.34ab	0.22 ± 0.00b	113.48 ± 0.11a	0.09 ± 0.00c

[a]The temperatures denoted in the dashed rectangle indicate the thermal transition peak temperature (T_p) and the calorific value represents enthalpy changes (ΔH). Different letters in the same column mean significant differences ($P < 0.05$).

that the fibrous structure was formed after the cooling zone so that the lipid was fully integrated into the protein network structure.[21]

3.3. DSC Analysis. The DSC data on peanut protein samples are summarized in Table 2 and shown in Figure 3a. Two endothermic peaks appeared in the DSC curves of each sample, corresponding to the denaturation of conarachin (low-temperature endotherm) and arachin (high-temperature endotherm).[28] Figure 3a shows that after the treatment in the mixing zone, the endothermic peak of conarachin decreased greatly as the ΔH value decreased significantly ($P < 0.05$) from 0.48 to 0.16 J g^{-1}, indicating that the molecular chains of conarachin were opened to a greater extent. However, after passing through the mixing zone, the T_p and ΔH values of arachin both decreased significantly ($P < 0.05$). This indicated that although the arachin was below its denaturation temperature, its molecular chains still unfolded, making it more flexible.[29]

In the melting zone, there was no significant ($P < 0.05$) difference between the thermal transition properties of conarachin with those in the mixing zone, which also confirmed the complete unfolding of conarachin. In the melting zone, the endothermic peak of arachin was greatly reduced, as shown by a significant decrease ($P < 0.05$) in the T_p and ΔH values. This phenomenon implies that the extreme reaction conditions, especially the high temperature in the melting zone, could promote the complete unfolding of the arachin molecular chains.[30] The large gels (Figure 2b,c) may have formed mainly through the aggregation of the unfolded arachin molecular chains but not those of conarachin.

Surprisingly, the ΔH value of conarachin increased significantly ($P < 0.05$) from 0.20 J g^{-1} to about 0.53 J g^{-1} in the die, which suggested that the conarachin had refolded. The decreased T_p value of conarachin in the die was also understandable given that the molecular chains of conarachin are known to become flexible or degraded after passing through the die.[29] Similarly, the T_p value of arachin decreased significantly ($P < 0.05$) in the die, suggesting a complete unfolding of its molecular chains. Therefore, after passing through the die, the conarachin and arachin both became flexible with active sites for aggregation being fully exposed, which created favorable conditions for their rearrangement in the subsequent extrusion zones.[31]

The T_p value of arachin increased significantly ($P < 0.05$) in the cooling zone and in the extrudate, which indicated that the aggregates of arachin had become more cross-linked (Figure 5).[32] The T_p value of conarachin increasing slightly, and the significant decrease ($P < 0.05$) in the ΔH value, indicated that the refolded conarachin molecular chains had been disrupted to a certain extent in the cooling zone. It can thus be concluded that conarachin and arachin exhibited different thermal transition behaviors during the high-moisture extrusion process and that arachin played a more important role than conarachin in the formation of the fibrous structure.

3.4. Thermal Gravimetric Analysis. Figure 3b shows that the mass loss of the raw material was approximately 2−3% lower than in the other zones at heating temperatures of 150, 250, and 350 °C. Therefore, the high-moisture extrusion process reduced thermal stability by degrading the protein amino acid residues.[33]

In general, there should be four main mass loss rate peaks in the DTG curve (Figure 3c).[18] The first peak at around 110 °C disappeared after the mixing zone, possibly because the unfolding of the protein molecular chains had led to an increase in the number of exposed hydrophobic groups, which could further decrease the capacity of the protein to bind with water.[34]

According to previous studies,[35] the second peak between 110 and 250 °C was mainly caused by the decomposition of the plasticizer and the cleavage of the covalent bonding between the peptide bonds of the amino acid residues. In the present study, plasticizer refers mainly to the lipids in the peanut protein powder. Table 3 shows that the second break temperature in the melting zone was significantly ($P < 0.05$) higher (3−4 °C) than in the previous extrusion zones but decreased significantly ($P < 0.05$) in the die and in the cooling zone. These results indicated that the protein−lipid interactions were enhanced in the melting zone by the unfolding of the protein molecular chains. However, the protein aggregation and the phase separation in the die were not conducive to protein−lipid interactions as mentioned earlier.[36] Interestingly, in the extrudate, the temperature went back to a significantly higher ($P < 0.05$) value (about 229.29 °C), which was also consistent with the AFM-IR results, showing that the lipids may have been fully integrated into the protein network structure, which then improved the thermal stability.

The third break between 250 and 350 °C was probably due to the cleavage of S−S, O−N, and O−O linkages in the protein molecules.[18,35] In the present study, the break temperature at around 310 °C in the melting zone decreased significantly ($P < 0.05$), indicating the cleavage of intramolecular disulfide bonds (Table 5).[18]

The fourth break after 350 °C was mainly due to the complete decomposition of the protein molecules. Figure 3c shows that the peak strength between 350 and 380 °C decreased mostly after the mixing zone, indicating that the extrusion process had accelerated the degradation of protein molecules.[36] Also, outside the extruder barrel (the die, cooling zone, and extrudate), the fourth break temperature was

DOI: 10.1021/acs.jafc.9b02711
J. Agric. Food Chem. 2019, 67, 10713−10725

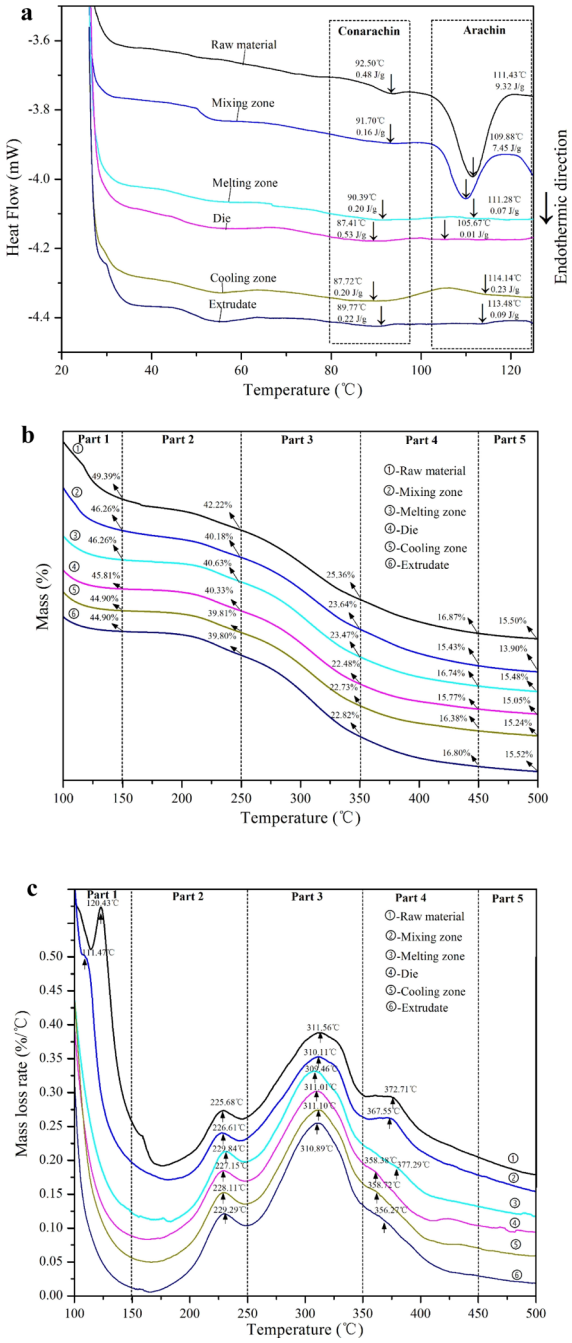

Figure 3. Thermal transition and decomposition properties of the peanut protein after extruding in each zone during the high-moisture extrusion process. (a) DSC endotherms. (b) TG curves. (c) DTG curves.

significantly lower ($P < 0.05$) by about 10−20 °C than that in the extruder barrel (mixing zone and melting zone) and of the raw material. These findings demonstrated that the protein structure had become more fragile during the molecular rearrangement occurring after passing through the die.

3.5. Rheological Properties. Figure 4a,b and Table 4 present the steady shear flow curves and the power law equation fitting results of the protein sample dispersions (20% w/w) at different shear rates. As shown in Table 4, the apparent viscosity and K value of the raw material, protein samples in the mixing zone and melting zone decreased gradually. However, no significant changes of the apparent

Table 3. Thermal Decomposition Properties of Peanut Protein during the High-Moisture Extrusion Process[a]

extrusion zones	part 1 (30−150 °C)		part 2 (150−250 °C)		part 3 (250−350 °C)		part 4 (350−450 °C)		part 5 (450−500 °C)
	peak 1/°C	mass (150 °C)/%	peak 2/°C	mass (250 °C)/%	peak 3/°C	mass (350 °C)/%	peak 4/°C	mass (450 °C)/%	mass (500 °C)/%
raw material	120.43 ± 0.48a	49.39 ± 2.52a	225.68 ± 0.92d	42.22 ± 2.40a	311.56 ± 1.40a	25.36 ± 1.02a	372.71 ± 2.18a	16.87 ± 0.06a	15.50 ± 0.12a
mixing zone	111.47 ± 0.32b	46.26 ± 0.06b	226.61 ± 0.60cd	40.18 ± 0.06a	310.11 ± 0.99ab	23.64 ± 0.04b	367.55 ± 0.10b	15.43 ± 0.18c	13.90 ± 0.02b
melting zone	-	46.05 ± 0.87b	229.84 ± 0.00a	40.63 ± 0.36a	309.46 ± 0.68b	23.47 ± 0.39b	377.65 ± 0.51a	16.74 ± 0.36a	15.48 ± 0.32a
die	-	45.81 ± 0.65b	227.15 ± 0.14bc	40.33 ± 1.04a	311.01 ± 0.06ab	22.48 ± 0.05b	358.38 ± 0.50cd	15.77 ± 0.37bc	15.05 ± 0.15a
cooling zone	-	44.90 ± 0.18b	228.11 ± 0.35b	39.81 ± 0.17a	311.10 ± 0.26ab	22.73 ± 0.25b	358.72 ± 0.58c	16.38 ± 0.18ab	15.24 ± 0.15a
extrudate	-	44.90 ± 0.34b	229.29 ± 0.09a	39.80 ± 0.33a	310.89 ± 0.17ab	22.82 ± 0.19b	356.27 ± 0.24d	16.80 ± 0.40a	15.52 ± 0.27a

[a]"-" means that the indicator is not detected; different letters in the same column mean significant differences ($P < 0.05$).

DOI: 10.1021/acs.jafc.9b02711
J. Agric. Food Chem. 2019, 67, 10713−10725

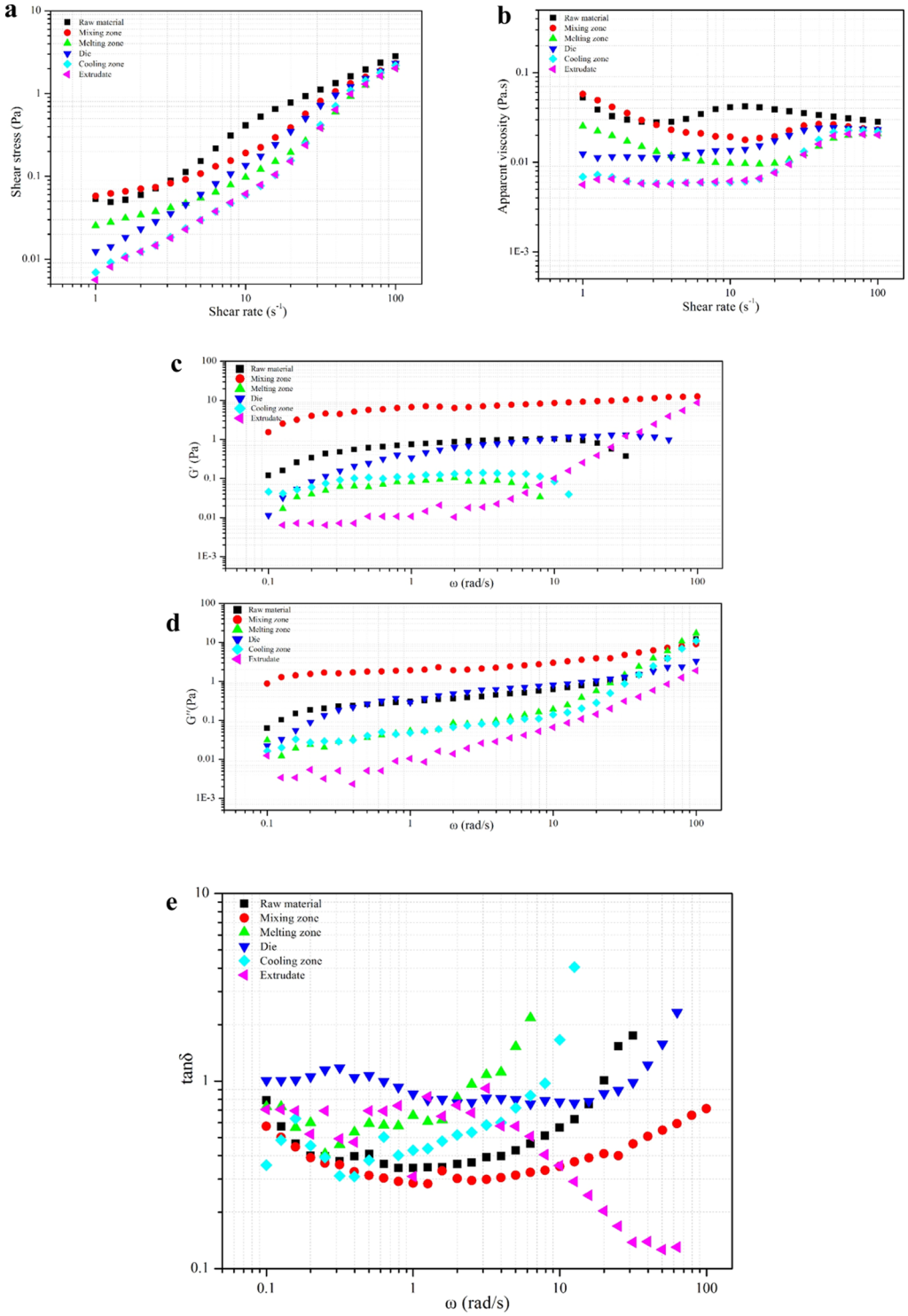

Figure 4. Rheological properties of dispersions containing 20% (w/w) peanut protein biomass after extruding in each zone during the high-moisture extrusion process. (a) Shear stress−shear rate relationship. (b) Variation of apparent viscosity with shear rate. (c) Variation of storage modulus (G'), (d) variation of loss modulus (G''). (e) tan δ with frequency.

viscosity and K value were found for the protein samples passing through the die and the cooling zone to form the extrudate. This means that when the protein molecular chains unfolded in the extruder barrel and rearranged in the die and the cooling zone, the protein structure became more stable to resist shearing by the rheometer.[37] Naturally, the apparent viscosity decreased when the protein denatured as the curves of the raw material and the mixing zone were higher than those in other zones. It notes that the apparent viscosity of the samples in the die seems higher than that of the previous zone (melting zone) and subsequent zone (cooling zone), indicating that association or reaggregation of the denatured proteins occurred in the die.[20,32] After the die, the cross-linking of the proteins and the interactions between protein and other components proceeded to form a fragile fibrous structure,

DOI: 10.1021/acs.jafc.9b02711
J. Agric. Food Chem. 2019, 67, 10713−10725

Table 4. Power Law Equation Fitting Results of Steady Shear Flow Curves of Peanut Protein during the High-Moisture Extrusion Process[a]

extrusion zones	power law equation: $\tau = K\cdot\gamma^n$		
	K ($\times 10^{-3}$ Pa·s^n)	n	R^2
raw material	36.75 ± 0.35a	0.97 ± 0.01c	0.988
mixing zone	19.40 ± 4.67b	1.02 ± 0.06c	0.969
melting zone	14.75 ± 0.07b	0.97 ± 0.02c	0.942
die	9.45 ± 0.49c	1.21 ± 0.02b	0.995
cooling zone	4.20 ± 0.28d	1.31 ± 0.01a	0.972
extrudate	4.20 ± 0.14d	1.32 ± 0.02a	0.981

[a]Different letters in the same column mean significant differences ($P < 0.05$).

which greatly decreased the resistance to shearing motion and hence decreased the apparent viscosity with a higher n value.[19]

G' represents a measure of elastic response of the material, whereas G'' is a measure of the viscous response; tan δ is a factor that measures damping. Protein sample dispersion with a higher tan δ than 1 shows a more liquid-like behavior, whereas that of lower tan δ than 1 can maintain its viscoelastic character to a greater extent.[38] In our study, low viscoelastic moduli were observed. It can be seen from Figure 4c,d that both G' and G'' increased with the increase in the angular frequency. For all dispersions, G' was higher than G'' at a lower frequency, meaning the predominance of the elastic contribution compared to the viscous one.[19,39] The raw material and the protein samples in the die had similar G' and G'' curves, but the tan δ of the protein samples in the die was much higher than that of the raw material, showing a much stronger liquid-like property because of the improvement of the protein (arachin) molecular chain flexibility in the die according to the DSC data previously. For the mixing zone and the extrudate, although both G' and G'' increase as the frequency increased, tan δ showed the opposite result (Figure 4e). The clear increase of tan δ in the mixing zone indicated that the chemical cross-linking in the raw material has not been seriously disrupted.[20] The clear decrease of tan δ in the extrudate indicated that after reaggregation and the formation of the fibrous structure, the protein structure became more fragile as mentioned preciously. However, with the increase in frequency, the G' curves of the melting zone and the cooling zone were interrupted (Figure 4c) as a consequence of the unfolding and cross-linking of the protein molecules in these two zones.[40] It can be concluded from the rheological data that the linear arrangement of protein (melting zone and cooling zone) is the key process for the reticulated fibrous structure. However, it is on the contrary when the proteins are in the initial state, arranged or aggregated like a cluster with higher G'' and apparent viscosity (raw material, mixing zone, and the die).

3.6. Protein−Protein Interactions. To investigate the protein−protein interactions, we first analyzed the protein solubilities in eight buffer systems (Figure 5). Of these extraction solutions, P solubilized the lowest amount of proteins in all the zone samples tested, with the solubility decreasing significantly ($P < 0.05$) in the extruder barrel because of the denaturation and aggregation of the protein molecules. After passing through the extruder barrel (mixing and melting zones), the protein solubility in P + U, P + M, P + S, P + U + M, and P + U + S decreased significantly ($P < 0.05$). However, in the cooling zone, the protein solubilities in

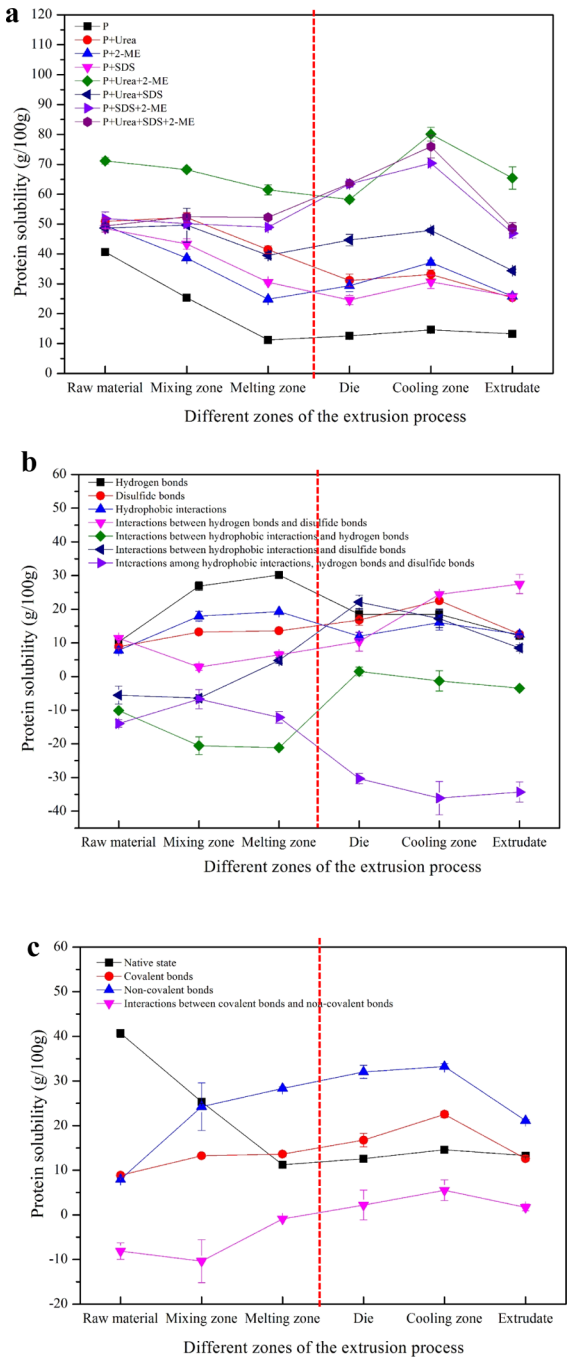

Figure 5. Protein solubility of the samples collected from different extrusion zones in eight buffer systems. (a) Protein solubility in different buffer systems. (b) Specific chemical bonds and their interactions. (c) Chemical cross-linking.

P, P + M, P + S, P + U + M, P + S + M, and P + U + S + M increased significantly ($P < 0.05$). These interesting results showed that the force maintaining the initial protein structure had been disrupted in the extruder barrel. Then, new forces had formed when the protein passed through the die and particularly in the cooling zone. However, the protein solubilities in the extrudate were significantly ($P < 0.05$) lower than those in the cooling zone, probably because of the prolonged fractionation during this process.[41]

The relative importance of each specific chemical bond and their interactions were determined by analyzing the average

DOI: 10.1021/acs.jafc.9b02711
J. Agric. Food Chem. 2019, 67, 10713−10725

Table 5. Secondary Structure of Peanut Protein during the High-Moisture Extrusion Process[a]

extrusion zones	secondary structure ratios/%				
	α-helix	β-sheet	β-turn	random coil	α-helix/β-sheet
raw material	22.59 ± 1.36d	30.97 ± 1.92cd	31.74 ± 3.23a	14.70 ± 0.05a	0.73 ± 0.01bc
mixing zone	37.93 ± 0.24bc	38.82 ± 2.22b	8.47 ± 0.70c	14.78 ± 1.27a	0.98 ± 0.06b
melting zone	33.77 ± 0.46c	47.82 ± 2.99a	13.86 ± 4.12c	4.55 ± 1.59b	0.71 ± 0.05c
die	35.84 ± 1.82c	45.58 ± 0.41a	12.98 ± 2.13c	5.59 ± 0.10b	0.79 ± 0.03bc
cooling zone	45.05 ± 2.84a	36.26 ± 3.19bc	15.11 ± 3.78bc	3.59 ± 2.24b	1.24 ± 0.03a
extrudate	42.84 ± 4.44ab	30.52 ± 1.62d	21.49 ± 2.31b	5.15 ± 0.51b	1.41 ± 0.22a

[a]Different letters in the same column mean significant differences ($P < 0.05$).

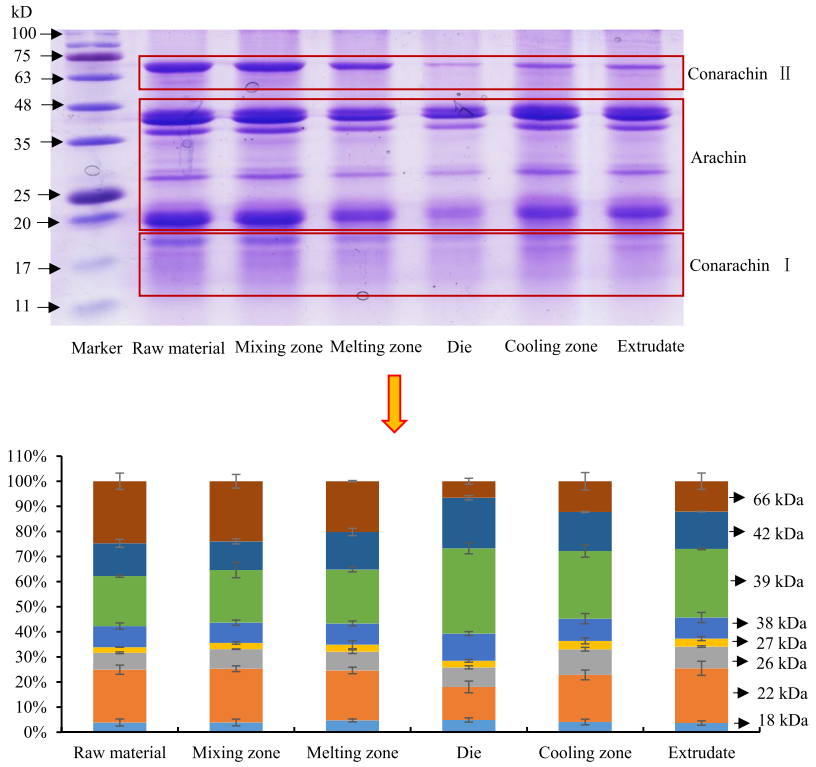

Figure 6. Molecular weight distribution of peanut protein during the high-moisture extrusion process.

value of protein solubility in the eight extraction solutions. The calculated values of solubilization because of the effect of S + U and S + M + U were negative, showing that urea solution can not only break hydrogen bonds but also disturb hydrophobic interactions,[9] resulting in repeating the calculations for analyzing hydrogen bonds and hydrophobic interactions. The negative solubility value for the analysis of interactions between hydrophobic interactions and disulfide bonds was also caused by the instability of the ionic bond that can be also broken by SDS.

Figure 5b shows that the amount of soluble protein caused by the effects of U, M, S, and S + M increased sharply ($P < 0.05$) in the extruder barrel. Thus, more hydrogen bonds formed when mixing the protein with water. This also proved that as well as the unfolding of protein molecular chains in the extruder barrel, more hydrophobic groups were exposed and more intermolecular disulfide bonds were formed.[34] Interactions between hydrogen bonds and disulfide bonds decreased significantly ($P < 0.05$) in the extruder barrel, which also illustrated that the force maintaining the initial structure of peanut protein could be disrupted as the protein molecular chains unfolded.[29]

In the die, the amount of soluble protein caused by the effects of U, M, and S decreased significantly ($P < 0.05$), but increased significantly ($P < 0.05$) from the effects of U + M, S + M, and S + U. These results indicated that when the protein passed through the narrow-caliber die, it shifted hydrogen bonds, disulfide bonds, and hydrophobic interactions to more complex interactions.

In the cooling zone, the amount of proteins bonded by M, S, and U + M increased significantly ($P < 0.05$), but decreased significantly ($P < 0.05$) for S + M. This suggested that the protein molecules were cross-linked mainly by disulfide bonds and the interactions between hydrogen bonds and disulfide bonds in the cooling zone.[29] The increase in hydrophobic interactions found in the cooling zone may be caused by the enhancement of protein−lipid interactions as also shown by the AFM-IR data.

In the extrudate, the number of protein molecules bonded by U, M, S, and S + M decreased significantly ($P < 0.05$), but Table 5 shows that a large number were bonded by U + M. Thus, it can be suggested that the interactions between hydrogen bonds and disulfide bonds were the main force maintaining the fibrous structure in the extrudate.

DOI: 10.1021/acs.jafc.9b02711
J. Agric. Food Chem. 2019, 67, 10713−10725

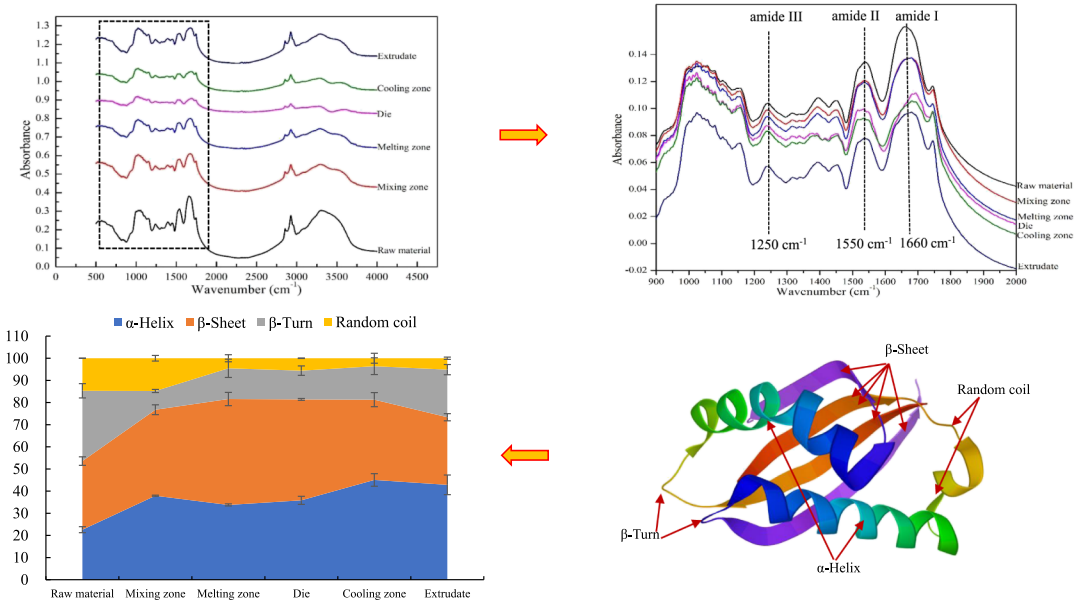

Figure 7. Changes in secondary structure of peanut protein during the high-moisture extrusion process determined by FTIR.

3.7. Molecular Weight Distribution. Figure 6 shows the SDS-PAGE profiles of peanut protein during the extrusion process in the presence of β-mercaptoethanol. Eight bands were exhibited ranging in molecular weight from 18 to 64 kDa for the peanut protein samples in each extrusion zone. The protein subunits in the mixing zone were almost the same as those in the raw material, showing that the protein had not been degraded in the mixing zone.

As the protein passed through the melting zone, the band at 66 kDa became narrow and the band density at 42 kDa increased significantly ($P < 0.05$) (Table S5). Therefore, the extreme reaction conditions in the melting zone led to the degradation of conarachin II and the aggregation of arachin.[22]

Because of insolubilization, the band color of the protein in the die was clearly lighter than those in the raw material, and the mixing, and melting zones.[42] In the die, the density of the bands at 66 and 22 kDa decreased significantly ($P < 0.05$), but increased significantly ($P < 0.05$) for the bands at 42 and 39 kDa. This suggested that the basic arachin (molecular weight, 22 kDa) had been cross-linked by the disulfide bonds in the die,[43] whereas the conarachin was degraded and Maillard reactions occurred, thus forming insoluble substances.[9]

In the cooling zone, the density of the bands at 42 and 39 kDa decreased significantly ($P < 0.05$), but increased significantly ($P < 0.05$) for the bands at 26 and 22 kDa ($P < 0.05$). This may have been caused by the degradation of arachin, which also illustrated that the fragile structure of the protein formed in the cooling zone can easily be disrupted when subjected to grinding.[18] No significant differences in the molecular weight distribution were found between material from the cooling zone and the extrudate. Throughout the extrusion process, there were no significant changes in the band density at 27 and 18 kDa, indicating that these protein fractions did not contribute to the formation of the fibrous structure.[42]

3.8. Changes in the Secondary Structure of Peanut Protein. FTIR is a highly sensitive technique that is suitable for investigating protein conformation.[44] The FTIR data from the peanut protein samples are summarized in Table 5 and shown in Figure 7. The amide I region (1700−1600 cm^{-1}) of the FTIR spectrum was selected for a detailed investigation, because it provides most information on the secondary structure of proteins.[45] The changes in the secondary structure were obtained by deconvolution of the amide I bands with a second derivative fitting then expressed as a percentage of the corresponding area by ratio to the total amide I band area.

Table 5 shows that the α-helix and β-sheet ratios both increased significantly ($P < 0.05$) in the mixing zone compared with the raw material but the ratio of β-turn decreased significantly ($P < 0.05$). This indicated that the gradual unfolding of protein molecular chains, mainly conarachin, accompanied by the hydrogen bonds formed in the mixing zone would lead to the disruption of the β-turn structure, and simultaneously promote the formation of more α-helix and β-sheet structures.[40]

In the melting zone, the β-sheet ratio increased significantly ($P < 0.05$) with a significant ($P < 0.05$) reduction in the random coil structure, results which contrasted with previous studies.[40] This unexpected result suggested that, during the high-moisture extrusion process, the combined effect of high temperature, shear force, and pressure in the melting zone promoted the complete unfolding of the protein molecular chains (conarachin and arachin) and made them more orderly.[46,47]

When the protein passed through the die, no significant changes in the secondary structure were found. Subsequently, in the cooling zone, the α-helix ratio increased significantly ($P < 0.05$), whereas the β-sheet ratio decreased significantly ($P < 0.05$). This suggested that the degradation of conarachin (as β-sheet is the dominant structure of conarachin) occurred in the cooling zone.[47] The β-sheet ratio also continued to decrease significantly ($P < 0.05$) in the extrudate, but the β-turn ratio increased significantly ($P < 0.05$). This interesting result suggested that the rearrangement of protein molecules had promoted the transformation of β-sheet to β-turn, which might be attributed to hydrogen bonds being weakened and even cleaved.[40]

The α-helix to β-sheet ratio can be used to indicate the flexibility of protein molecules, and their susceptibility to extrusion conditions.[34] In the present study, the α-helix to β-

DOI: 10.1021/acs.jafc.9b02711
J. Agric. Food Chem. 2019, 67, 10713−10725

sheet ratio was significantly higher ($P < 0.05$) in the mixing zone (0.98) than in the raw material (0.73) (Table 5). This indicated that the protein molecules had swollen when water entered the mixing zone, instead of completely unfolding.

Subsequently, in the melting zone and the die, the α-helix to β-sheet ratio decreased significantly ($P < 0.05$), to the same value as that of the raw material. This suggested that the protein structure had become more flexible alongside the complete unfolding of the protein molecular chains.

However, a significant increase ($P < 0.05$) in the α-helix to β-sheet ratio was seen both in the cooling zone and the extrudate. This result was consistent with the DSC and thermal gravimetric analysis data, which suggested that the unfolded protein molecular chains had been rearranged and had returned to a fragile wire cluster structure (fibrous structure) after passing through the die.[40]

■ ASSOCIATED CONTENT

Supporting Information

The Supporting Information is available free of charge on the ACS Publications website at DOI: 10.1021/acs.jafc.9b02711.

> Extrusion equipment for producing high-moisture extruded-texturized peanut protein and "double green" meat substitutes; high-moisture extrusion process for production of texturized peanut protein and "green" meat substitutes; screw configuration used for the high-moisture extrusion process; IR absorption peak of the protein powder, peanut protein isolate, and peanut lipid; physical and chemical characteristics of the peanut protein powder; protein solubility of extruded samples collected from different extrusion zones in different buffer systems; specific chemical bonds and the interactions of extruded samples collected from different extrusion zones; chemical cross-linking of the extruded samples collected from different extrusion zones; and molecular weight distribution ratio of peanut protein during the high-moisture extrusion process (PDF)

■ AUTHOR INFORMATION

Corresponding Author

*E-mail: wangqiang06@caas.cn. Phone: +86-10-62815837. Fax: +86-10-62815837.

ORCID

Qiang Wang: 0000-0002-2564-1491

Notes

The authors declare no competing financial interest.

■ ACKNOWLEDGMENTS

This research was supported by the National Key Research and Development Plan of China (2016YFD0400200), National Natural Science Foundation of China (31801487), and the Science and Technology Innovation Project of Chinese Academy of Agricultural Sciences (CAAS-ASTIP-201X-IAPPST). We are also grateful to Wen Shi who is the staff of Carl Zeiss (Shanghai) Co., Ltd. for the assistance of X-ray microscopy imaging.

■ REFERENCES

(1) Clark, J. H. Green biorefinery technologies based on waste biomass. *Green Chem.* **2019**, *21*, 1168−1170.

(2) Godfray, H. C. J.; Beddington, J. R.; Crute, I. R.; Haddad, L.; Lawrence, D.; Muir, J. F.; Pretty, J.; Robinson, S.; Thomas, S. M.; Toulmin, C. Food Security: The Challenge of Feeding 9 Billion People. *Science* **2010**, *327*, 812.

(3) Tilman, D.; Clark, M. Global diets link environmental sustainability and human health. *Nature* **2014**, *515*, 518−522.

(4) Hedenus, F.; Wirsenius, S.; Johansson, D. J. A. The importance of reduced meat and dairy consumption for meeting stringent climate change targets. *Clim. Change* **2014**, *124*, 79−91.

(5) Pietsch, V. L.; Emin, M. A.; Schuchmann, H. P. Process conditions influencing wheat gluten polymerization during high moisture extrusion of meat analog products. *J. Food Eng.* **2016**, *198*, 28−35.

(6) Zhang, J.; Liu, L.; Liu, H.; Yoon, A.; Rizvi, S. S. H.; Wang, Q. Changes in Conformation and Quality of Vegetable Protein during Texturization Process by Extrusion. *Crit. Rev. Food Sci. Nutr.* **2018**, 1−14.

(7) Wild, F.; Czerny, M.; Janssen, A. M.; Kole, A. P. W.; Zunabovic, M.; Domig, K. J. The evolution of a plant-based alternative to meat: From niche markets to widely accepted meat alternatives. *Agro Food Ind. Hi-Tech* **2014**, *25*, 45−49.

(8) Wang, Q. Quality Characteristics and Determination Methods of Peanut Raw Materials. In *Peanut Processing Characteristics and Quality Evaluation*; Wang, Q., Ed.; Springer: Singapore, 2018; pp 69−125.

(9) Chen, F. L.; Wei, Y. M.; Zhang, B. Chemical cross-linking and molecular aggregation of soybean protein during extrusion cooking at low and high moisture content. *LWT—Food Sci. Technol.* **2011**, *44*, 957−962.

(10) Yao, G.; Liu, K. S.; Hsieh, F. A New Method for Characterizing Fiber Formation in Meat Analogs during High-moisture Extrusion. *J. Food Sci.* **2004**, *69*, 303−307.

(11) Osen, R.; Toelstede, S.; Wild, F.; Eisner, P.; Schweiggert-Weisz, U. High moisture extrusion cooking of pea protein isolates: Raw material characteristics, extruder responses, and texture properties. *J. Food Eng.* **2014**, *127*, 67−74.

(12) Karunanithy, C.; Muthukumarappan, K.; Gibbons, W. R. Sequential extrusion-ozone pretreatment of switchgrass and big bluestem. *Appl. Biochem. Biotechnol.* **2014**, *172*, 3656−3669.

(13) Liu, K.; Hsieh, F.-H. Protein-protein interactions during high-moisture extrusion for fibrous meat analogues and comparison of protein solubility methods using different solvent systems. *J. Agric. Food Chem.* **2008**, *56*, 2681−2687.

(14) Dazzi, A.; Prater, C. B. AFM-IR: Technology and Applications in Nanoscale Infrared Spectroscopy and Chemical Imaging. *Chem. Rev.* **2017**, *117*, 5146−5173.

(15) Liu, Z.-H.; Qin, L.; Li, B.-Z.; Yuan, Y.-J. Physical and Chemical Characterizations of Corn Stover from Leading Pretreatment Methods and Effects on Enzymatic Hydrolysis. *ACS Sustainable Chem. Eng.* **2015**, *3*, 140−146.

(16) Zhang, J.; Liu, L.; Zhu, S.; Wang, Q. Texturisation behaviour of peanut-soy bean/wheat protein mixtures during high moisture extrusion cooking. *Int. J. Food Sci. Technol.* **2018**, *53*, 2535−2541.

(17) Fang, Y.; Zhang, B.; Wei, Y. Effects of the specific mechanical energy on the physicochemical properties of texturized soy protein during high-moisture extrusion cooking. *J. Food Eng.* **2014**, *121*, 32−38.

(18) Zhang, J.; Ying, D.; Wei, Y.; Zhang, B.; Su, X.; Li, S. Thermal transition and decomposition properties of pH- and phosphate-induced defatted soybean meals. *J. Therm. Anal. Calorim.* **2017**, *128*, 699−706.

(19) Chang, Y.-y.; Li, D.; Wang, L.-j.; Bi, C.-h.; Adhikari, B. Effect of gums on the rheological characteristics and microstructure of acid-induced SPI-gum mixed gels. *Carbohydr. Polym.* **2014**, *108*, 183−191.

(20) Manoi, K. Physico-chemical properties of whey protein concentrates. Ph.D. Thesis, Cornell University, USA, 2009.

(21) Liu, K.; Hsieh, F.-H. Protein-Protein Interactions during High-Moisture Extrusion for Fibrous Meat Analogues and Comparison of Protein Solubility Methods Using Different Solvent Systems. *J. Agric. Food Chem.* **2008**, *56*, 2681−2687.

(22) He, X.-H.; Liu, H.-Z.; Liu, L.; Zhao, G.-L.; Wang, Q.; Chen, Q.-L. Effects of high pressure on the physicochemical and functional

properties of peanut protein isolates. *Food Hydrocolloids* **2014**, *36*, 123−129.
(23) Pal, D.; Tripathy, R. K.; Teja, M. S.; Kumar, M.; Banerjee, U. C.; Pande, A. H. Antibiotic-free expression system for the production of human interferon-beta protein. *Biotech* **2018**, *8*, 36.
(24) Thiébaud, M.; Dumay, E.; Cheftel, J. C. Influence of process variables on the characteristics of a high moisture fish soy protein mix texturized by extrusion cooking. *LWT—Food Sci. Technol.* **1996**, *29*, 526−535.
(25) Alzagtat, A. A.; Alli, I. Protein-lipid interactions in food systems: a review. *Int. J. Food Sci. Nutr.* **2002**, *53*, 249.
(26) Amenabar, I.; Poly, S.; Nuansing, W.; Hubrich, E. H.; Govyadinov, A. A.; Huth, F.; Krutokhvostov, R.; Zhang, L.; Knez, M.; Heberle, J. Structural analysis and mapping of individual protein complexes by infrared nanospectroscopy. *Nat. Commun.* **2013**, *4*, 2890.
(27) Osen, R.; Toelstede, S.; Eisner, P.; Schweiggert-Weisz, U. Effect of high moisture extrusion cooking on protein-protein interactions of pea (Pisum sativumL.) protein isolates. *Int. J. Food Sci. Technol.* **2015**, *50*, 1390−1396.
(28) Colombo, A.; Ribotta, P. D.; León, A. E. Differential Scanning Calorimetry (DSC) Studies on the Thermal Properties of Peanut Proteins. *J. Agric. Food Chem.* **2010**, *58*, 4434.
(29) Yue, H.-B.; Cui, Y.-D.; Shuttleworth, P. S.; Clark, J. H. Preparation and characterisation of bioplastics made from cottonseed protein. *Green Chem.* **2012**, *14*, 2009−2016.
(30) Denavi, G. A.; Pérez-Mateos, M.; Añón, M. C.; Montero, P.; Mauri, A. N.; Gómez-Guillén, C. Structural and functional properties of soy protein isolate and cod gelatin blend films. *Food Hydrocolloids* **2009**, *23*, 2094−2101.
(31) Guo, J.; Yang, X.-Q.; He, X.-T.; Wu, N.-N.; Wang, J.-M.; Gu, W.; Zhang, Y.-Y. Limited Aggregation Behavior of β-Conglycinin and Its Terminating Effect on Glycinin Aggregation during Heating at pH 7.0. *J. Agric. Food Chem.* **2012**, *60*, 3782−3791.
(32) Verbeek, C. J. R.; van den Berg, L. E. Extrusion Processing and Properties of Protein-Based Thermoplastics. *Macromol. Mater. Eng.* **2010**, *295*, 10−21.
(33) Chabba, S.; Matthews, G. F.; Netravali, A. N. "Green" composites using cross-linked soy flour and flax yarns. *Green Chem.* **2005**, *7*, 576−581.
(34) Wang, K.; Luo, S.; Cai, J.; Sun, Q.; Zhao, Y.; Zhong, X.; Jiang, S.; Zheng, Z. Effects of partial hydrolysis and subsequent cross-linking on wheat gluten physicochemical properties and structure. *Food Chem.* **2016**, *197*, 168−174.
(35) Latza, V.; Guerette, P. A.; Ding, D.; Amini, S.; Kumar, A.; Schmidt, I.; Keating, S.; Oxman, N.; Weaver, J. C.; Fratzl, P. Multi-scale thermal stability of a hard thermoplastic protein-based material. *Nat. Commun.* **2015**, *6*, 8313.
(36) Koch, L.; Emin, M. A.; Schuchmann, H. P. Influence of processing conditions on the formation of whey protein-citrus pectin conjugates in extrusion. *J. Food Eng.* **2017**, *193*, 1−9.
(37) Ren, L.; Zeng, X.; Sun, R.; Xu, J.-B.; Wong, C.-P. Spray-assisted assembled spherical boron nitride as fillers for polymers with enhanced thermally conductivity. *Chem. Eng. J.* **2019**, *370*, 166−175.
(38) da Silva, D. F.; de Souza Ferreira, S. B.; Bruschi, M. L.; Britten, M.; Matumoto-Pintro, P. T. Effect of commercial konjac glucomannan and konjac flours on textural, rheological and microstructural properties of low fat processed cheese. *Food Hydrocolloids* **2016**, *60*, 308−316.
(39) Senturk-Ozer, S.; Gevgilili, H.; Kalyon, D. M. Biomass pretreatment strategies via control of rheological behavior of biomass suspensions and reactive twin screw extrusion processing. *Bioresour. Technol.* **2011**, *102*, 9068−9075.
(40) Wang, Y.; Chen, Y.; Zhou, Y.; Nirasawa, S.; Tatsumi, E.; Li, X.; Cheng, Y. Effects of konjac glucomannan on heat-induced changes of wheat gluten structure. *Food Chem.* **2017**, *229*, 409−416.
(41) Zhao, G.; Liu, Y.; Zhao, M.; Ren, J.; Yang, B. Enzymatic hydrolysis and their effects on conformational and functional properties of peanut protein isolate. *Food Chem.* **2011**, *127*, 1438−1443.
(42) Osen, R.; Toelstede, S.; Eisner, P.; Schweiggert-Weisz, U. Effect of high moisture extrusion cooking on protein-protein interactions of pea (Pisum sativumL.) protein isolates. *Int. J. Food Sci. Technol.* **2015**, *50*, 1390−1396.
(43) Beck, S. M.; Knoerzer, K.; Sellahewa, J.; Emin, M. A.; Arcot, J. Effect of different heat-treatment times and applied shear on secondary structure, molecular weight distribution, solubility and rheological properties of pea protein isolate as investigated by capillary rheometry. *J. Food Eng.* **2017**, *208*, 66−76.
(44) Rasheed, F.; Kuktaite, R.; Hedenqvist, M. S.; Gällstedt, M.; Plivelic, T. S.; Johansson, E. The use of plants as a "green factory" to produce high strength gluten-based materials. *Green Chem.* **2016**, *18*, 2782−2792.
(45) Georget, D. M. R.; Belton, P. S. Effects of temperature and water content on the secondary structure of wheat gluten studied by FTIR spectroscopy. *Biomacromolecules* **2006**, *7*, 469−475.
(46) Qin, X.-S.; Luo, S.-Z.; Cai, J.; Zhong, X.-Y.; Jiang, S.-T.; Zhao, Y.-Y.; Zheng, Z. Transglutaminase-induced gelation properties of soy protein isolate and wheat gluten mixtures with high intensity ultrasonic pretreatment. *Ultrason. Sonochem.* **2016**, *31*, 590.
(47) Carbonaro, M.; Nucara, A. Secondary structure of food proteins by Fourier transform spectroscopy in the mid-infrared region. *Amino Acids* **2010**, *38*, 679−690.

DOI: 10.1021/acs.jafc.9b02711
J. Agric. Food Chem. 2019, 67, 10713−10725